RSC Advances

PAPER

View Article Online
View Journal | View Issue

Cite this: *RSC Adv.*, 2019, **9**, 11253

CoS_x/C hierarchical hollow nanocages from a metal–organic framework as a positive electrode with enhancing performance for aqueous supercapacitors†

Weibin Zhou,‡[ab] Peng Wang,‡[ab] Chunyang Li,[ac] Qinghong Huang,[c] Jing Wang,[c] Yusong Zhu,*[ac] Lijun Fu,*[ac] Yuhui Chen[ac] and Yuping Wu*[ac]

Benefiting from abundant redox chemistry and high electrochemical properties, metal sulfides have been broadly employed as electrode materials in supercapacitor systems. However, the predominant limitation in their performance, which arises from indifferent electron and ion dynamics for transportation and a rapid slash in capacitance, is of particular concern. Herein, we portray the cobalt sulfides/carbon (CoS_x/C) hierarchical hollow nanocages using ZIF-67 nanocrystals coated with carbon from resorcinol–formaldehyde (ZIF-67@RF) as a self-sacrificial template. The RF acted as a hard framework to prevent the hollow structure from breaking and was transformed to a carbon layer to enhance the charge transfer process. When used as positive electrodes in supercapacitor systems with aqueous electrolytes, the optimized CoS_x/C hierarchic hollow nanocages exhibited a considerable specific capacitance (618 F g^{-1} at 2 A g^{-1}), superior rate performance (83.6% capacitance retention of the initial capacity when the current density was amplified from 2 A g^{-1} to 50 A g^{-1}) and an extraordinary cycle stationarity along with an undiminished specific capacitance after 10 000 cycles. In this study, the meticulously designed hierarchical hollow structure that we conceived not only provides an outstanding electrochemical performance but also provides options for other related materials, such as various MOFs.

Received 15th February 2019
Accepted 16th March 2019

DOI: 10.1039/c9ra01167f

rsc.li/rsc-advances

1. Introduction

Surpassing secondary batteries such as lithium ion batteries, sodium ion batteries and other metal ion batteries in power density, supercapacitors (SCs) are reckoned as irreplaceable and practical energy storage devices.[1–5] Amidst them, electrical double layers capacitors (EDLCs) mainly store narrow energy,[6–8] and are composed of carbon-based materials involving graphene, activated carbon and carbon nanotubes (CNTs). However, conductive polymers,[9,10] metal oxides[11–13] and sulfides,[14–17] called pseudocapacitive materials, often demonstrate a relatively higher energy density, which is attributed to the fast absorption/desorption and redox reactions on the surface of active materials in supercapacitors. Therefore, advanced pseudocapacitive materials with an eminent electrochemical performance have become research hotspots in this field.

Among miscellaneous pseudocapacitive materials ,[8,18–21] the use of metal sulfides as bright electrode materials in supercapacitors (SCs) have dominated recent research discussions. Hence, the academic community has extensively explored metal sulfides in inner construction applications covering stoichiometric formulations, valence states and morphologies encompassing nanocrystalline morphologies and crystal frameworks, which enable them to deliver electro-chemical activities. Moreover, metal sulfides commonly offer more trivial electrical resistance as well as mechanically and thermally amended stability than their corresponding metal oxide counterparts.[22] These unparalleled characters ensure a better electrochemical performance as electrodes compared to many other materials, consisting of carbonaceous materials and metal oxides. For instance, after the solvothermal operation, a flower-like β-NiS with a hierarchical architecture was collected, and then presented a specific capacity of 513 F g^{-1} at 5 A g^{-1}.[23] In addition to nickel sulfides, electrode materials from cobalt sulfides are similarly utilized for SCs.

Hybrid CoS/graphene with a 3D network highlighted a prosperous specific capacitance and a remarkable capacity retention

[a]State Key Laboratory of Materials-oriented Chemical Engineering, School of Energy Science and Engineering, Nanjing Tech University, Nanjing 211816, China. E-mail: zhuys@njtech.edu.cn; l.fu@njtech.edu.cn; wuyp@fudan.edu.cn

[b]Institute of Advanced Materials (IAM), Nanjing Tech University, Nanjing 210009, China

[c]School of Energy Science and Engineering, Nanjing Tech University, Nanjing 211816, China

† Electronic supplementary information (ESI) available. See DOI: 10.1039/c9ra01167f

‡ Equal contribution.

of 82% when operated at 20 A g^{-1}.[24] Because metal ions and organic ligands can be combined to form a periodically poriferous structure, metal–organic frameworks (MOFs) were widely investigated for energy storage applications.[25–32] For instance, the hierarchical CoS double-shelled hollow nanoboxes derived from a zeolitic imidazolate framework-67 (ZIF-67) demonstrated a high specific capacitance, and subsequently retained 60% of the initial capacitance at 20 A g^{-1}.[33] However, the limited rate performance and cycling stability required further improvement.

Due to the intrinsic poor electrical conductivity of metal oxides, carbon-based materials including multi-wall, double-wall and single-wall carbon nanotubes (CNTs) and reduced graphene oxide (rGO) are usually added into metal oxides to enhance the charge transfer process.[34–37] Co_3O_4 *in situ* coating on CNTs were synthesized *via* a hydrothermal procedure and used as cathode materials in aqueous supercapacitors, which showed a specific capacity of 590 F g^{-1} at the ampere density of 15 A g^{-1} and a specific capacitance of 510 F g^{-1} at 100 A g^{-1}.[38] Metal sulfides, which have also been processed in this way, demonstrated a better electrochemical performance compared to their pristine counterparts.[39–41] rGO-CNT-Co_3S_4 nanocomposites were optimized by adjusting the rGO concentration and the ratio of rGO/CNTs. These nanocomposites showed an optimally high specific capacitance due to an enhanced charge transfer procedure.[42] Our previous study on the formation of the sandwich structures from rGO and cobalt sulfides also suggested that the addition of rGO had positive effects on the capacitance performance.[43,44] Nevertheless, many studies focused on the charge transfer among large-size samples, such as micron-sized metal oxides particles, thus ignoring the high charge transfer resistance inside these particles.

Herein, we designed a rational and versatile hierarchical hollow structure with cobalt sulfide nanoparticles having a diameter *ca.* 10 nm attached on the surface of the conductive hollow carbon layer. ZIF-67 coated with a RF layer was applied as a self-sacrificial template and subsequently transformed to the hierarchical hollow CoS_x/C nanocages. The RF coating layer not only supported and stabilized the hollow structure during the sulfurization process, but was transformed to a conductive carbon layer during heat treatment to enhance the electrochemical performance as a positive electrode in aqueous supercapacitors. Due to the combination of the hollow structure and the conductive carbon shell, the resulting materials showed a superb rate performance and dramatically wonderful cycling stability. It is believed that this synthesis method and the unique hierarchical hollow structure could be extended to other related materials, such as various MOFs.

2. Experimental section

2.1 Preparation of ZIF-67@RF

All chemicals were obtained commercially and were used without additional purification. ZIF-67 was devised as the following: 2-methylimidazole (2-MI, 410 mg) and cobalt nitrate hexahydrate ($Co(NO_3)_2 \cdot 6H_2O$, 294 mg) were added to a 10 mL and 30 mL solvent mixture of methanol and ethanol with the volume ratio of 1 : 1. Then, the former solution was poured into the later solution under vigorous stirring for 15 min and then, the mixture was kept motionless for 24 h. The product was obtained by suction filtration and washed with methanol three times, followed by drying at 60 °C overnight.

ZIF-67@RF was prepared in line with the previous study:[45] 0.2 g of ZIF-8, 14 mL of deionized water and 6 mL of ethanol were mixed by ultrasonic treatment and stirred at room temperature. After 30 min, 0.23 g of cetyltrimethylammonium bromide (CTAB), 0.035 g of resorcinol and 0.1 mL of ammonium hydroxide were added in series. After another 30 min, 0.06 mL of a formaldehyde solution was added again. After 8 h, the resulting ZIF-67@resorcinol–formaldehyde (ZIF-67@RF) was achieved by washing with deionized water for 5 times. To change the RF content in ZIF-67@RF, the amount of both the resorcinol and formaldehyde solution was decreased to 1/2 and 1/4 without any other changes.

Hierarchical hollow CoS_x/C nanocages were compounded *via* the solvothermal method. The obtained ZIF-67@RF (100 mg) was dispersed in 30 mL of ethanol solution by ultrasonic treatment, followed by the addition of thioacetamide (TAA, 150 mg) and stirring the mixture for 30 min. Then, the mixture was transferred to a Teflon-lined stainless-steel autoclave, which was subsequently heated at 120 °C for 4 h. After naturally cooling to room temperature, the prepared black precipitate was separated by filtration, washed with ethanol 3 times and dried in an oven. Finally, the as-prepared sample was annealed at 575 °C under nitrogen for 2 h at a ramping rate of 2 °C min^{-1}. The final samples were denoted as CoS_x/C-1, CoS_x/C-2 and CoS_x/C-3, while the carbon or RF content increased gradually. In term of the pristine CoS_x, the synthesis procedure was the same except for that ZIF-67@RF was replaced with ZIF-67.

2.2 Material characterizations

Data on the morphology and structure of the samples were recorded using a field-emission scanning electron microscope (FESEM and JSM-7800F) and a high-resolution transmission electron microscope (HR-TEM, Tecnai 20UTwin) affiliated X-ray energy dispersive spectrometry (EDS). To characterize the structure and measure the chemical elements in the specimen, many instruments were incorporated, including an X-ray diffraction (XRD) (Rigaku D/Max-KA diffractometer with Cu Kα radiation, $\lambda = 1.5418$ Å), a Raman spectroscope (WITEC Alpha300M+), a thermogravimetric (TG)-differential scanning calorimeter (DSC, Netzsch STA 449 F5) and a Fourier-transform infrared spectroscope (FTIR) (Bruker ALPHA).

2.3 Electrochemical measurements

Electrochemical metrics were implemented in a three-electrode system, where a nickel mesh impersonated as the counter electrode, a saturated calomel electrode (SCE) acted as the reference electrode and an aqueous solution dissolved with 1 M KOH represented part of the electrolyte. After the commixture of the obtained samples with poly-(tetrafluoroethylene) (PTFE) and acetylene black in a proportion of 8 : 1 : 1 by weight and

the result was rolled into a thin film, the working electrode was achieved. After drying, a slice weighing *ca.* 2 mg was crushed into a nickel mesh, which represented the working electrode. Particularly, the mass loading for CoS_x, CoS_x/C-1, CoS_x/C-2 and CoS_x/C-3 was about 2 mg, which was precisely weighed prior to testing. In accordance with our former reports,[46] an electrochemical working station (CHI 660C) regulated the aggregation on the metrics of cyclic voltammograms (CV), electrochemical impedance spectroscopy (EIS) and charge–discharge surveying, while a Land CT2001A battery program-controlled test system (Land, Wuhan, China) recorded all the data during the cycling progress.

3. Result and discussion

The strategy for synthesizing the hierarchical hollow CoS_x/C nanocages is schematically depicted in Fig. 1 and the specifics are outlined in the experimental section. The obtained ZIF-67 with an average diameter of 200–400 nm has a smooth exterior surface, showing a typical rhombic dodecahedron shape, as shown in Fig. 2a. ZIF-67 nanocrystals could be coated by the RF due to the H-bonding from the ZIF-67 nanocrystals and the hydroxyl groups from RF. It can be clearly seen that the surface of ZIF-67@RF was rougher than that of the ZIF-67 nanocrystals and some RF flakes could be identified as shown in Fig. 2b. In order to confirm that the RF was covered on ZIF-67 during the

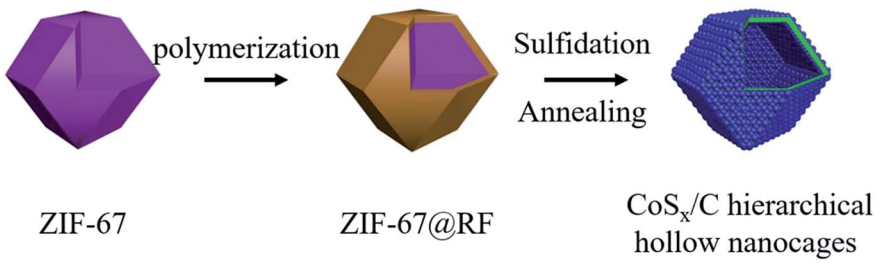

Fig. 1 Schematic for the synthesis of the CoS_x/C hierarchical hollow nanocages.

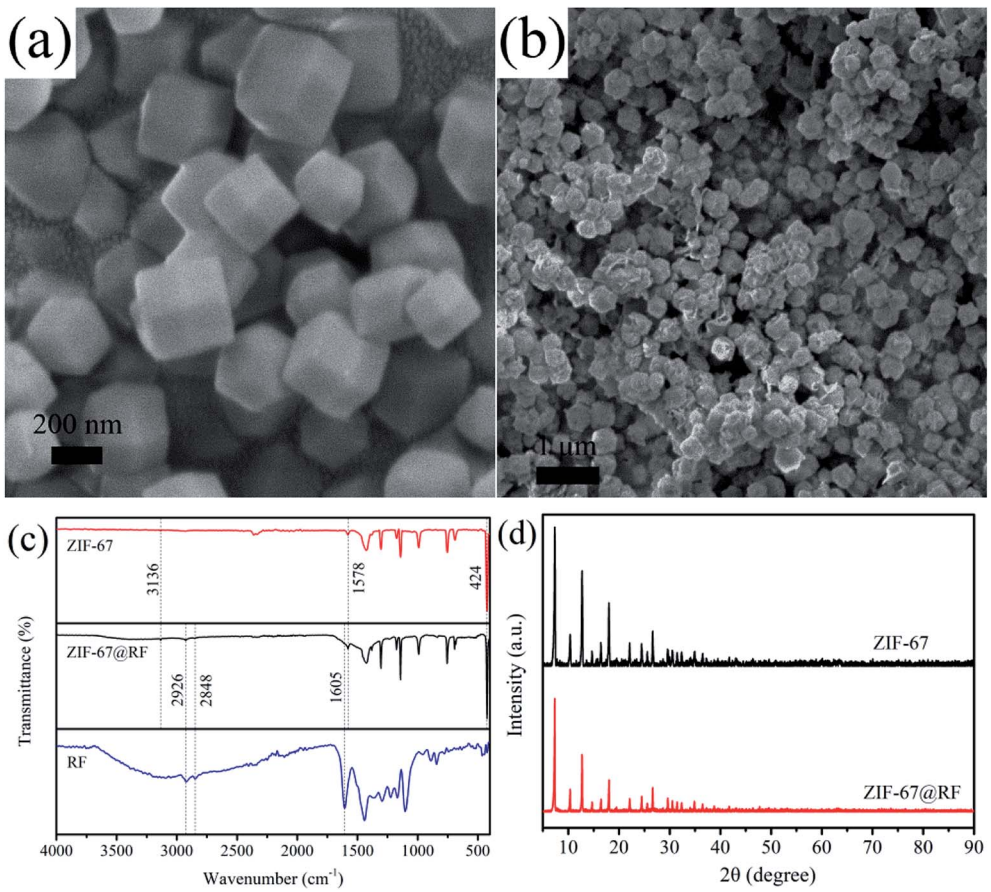

Fig. 2 SEM images of (a) ZIF-67 and (b) ZIF-67@RF. (c) FTIR spectra of ZIF-67, ZIF-67@RF and RF. (d) XRD patterns of ZIF-67 and ZIF-67@RF.

polymerization process, ZIF-67@RF was acidified with 1 M HCl for 30 min. The resulting dull yellow product showed a hollow shell maintaining the shape of ZIF-67 (Fig. S1a†). To compare the difference in functional groups on the surface between ZIF-67, ZIF-67@RF and the RF hollow shell, the FTIR spectra were recorded, as shown in Fig. 2c. The band at 1578 cm^{-1} was attributed to the stretching of the C=N bond, while the band at 3136 cm^{-1} was attributed to the stretching vibration of C–H from the aliphatic chain. Particularly, the band located at 424 cm^{-1} came from the stretching of the Co=N bond. The bands at 2929 and 2848 cm^{-1} were assigned to the CH_2 stretching and bending vibrations, respectively, whereas the band at 1605 cm^{-1} was assigned to the aromatic ring stretches. The results confirmed that ZIF-67 and RF coexisted and were blended effectively in ZIF-67@RF. Powder X-ray diffraction (XRD) patterns for both ZIF-67 and ZIF-67@RF are displayed in Fig. 2d, showing that the typical ZIF topologies are in agreement with previous reports.[47]

During the subsequent sulfurization process, the Co ion that dissociated from the ZIF-67 nanocrystals reacted with S^{2-} hydrolyzed from TAA, which resulted in cobalt sulfides.[48] In particular, the RF coating layer was supposed to act as the hard framework to form the hollow nanocages during the sulfurization process when the obtained cobalt sulfides nanoparticles could attach to the layer. The RF coating layer contained in the hollow nanocages was *in situ* transformed to a high-conductivity carbon layer after the heat treatment. To identify the positive influence that the RF coating layers exerted on the morphology of the ultimate products, various ZIF-67@RF samples with dissimilar proportion of RF were yielded after the same operation. These various samples were named CoS_x/C-1, CoS_x/C-2 and CoS_x/C-3, with a gradual increase in the RF content. As shown in Fig. 3, CoS_x without the RF coating layer was irregular and aggregated (Fig. 3a). A few broken hollow nanocages were recognized in CoS_x/C-1 (Fig. 3b), while the hollow structure remained unbroken and uniform for CoS_x/C-2 (Fig. 3c and Fig. S1b and c†) and CoS_x/C-3 (Fig. 3d). This distinct trend indicates that the RF coating layer effectively promoted the formation of the hierarchical hollow nanocages.

A closer inspection of Fig. 4 evidences the XRD patterns of CoS_x, CoS_x/C-1, CoS_x/C-2 and CoS_x/C-3. At the limit of the resolution ratio for our X-ray diffractometer, the XRD pattern of CoS_x/C-1 was more correlated with that of CoS_x/C-2 and CoS_x/C-3 compared with that of pristine CoS_x, illustrating negligible influence on the framework of the cube from the incorporation of carbon layer. All examples showed that the featured peaks of the (311) and (440) planes originated from Co_9S_8 (JCPDS card no. 19-0364) at 2θ values of 39.5° and 52.0°, labeled with purple

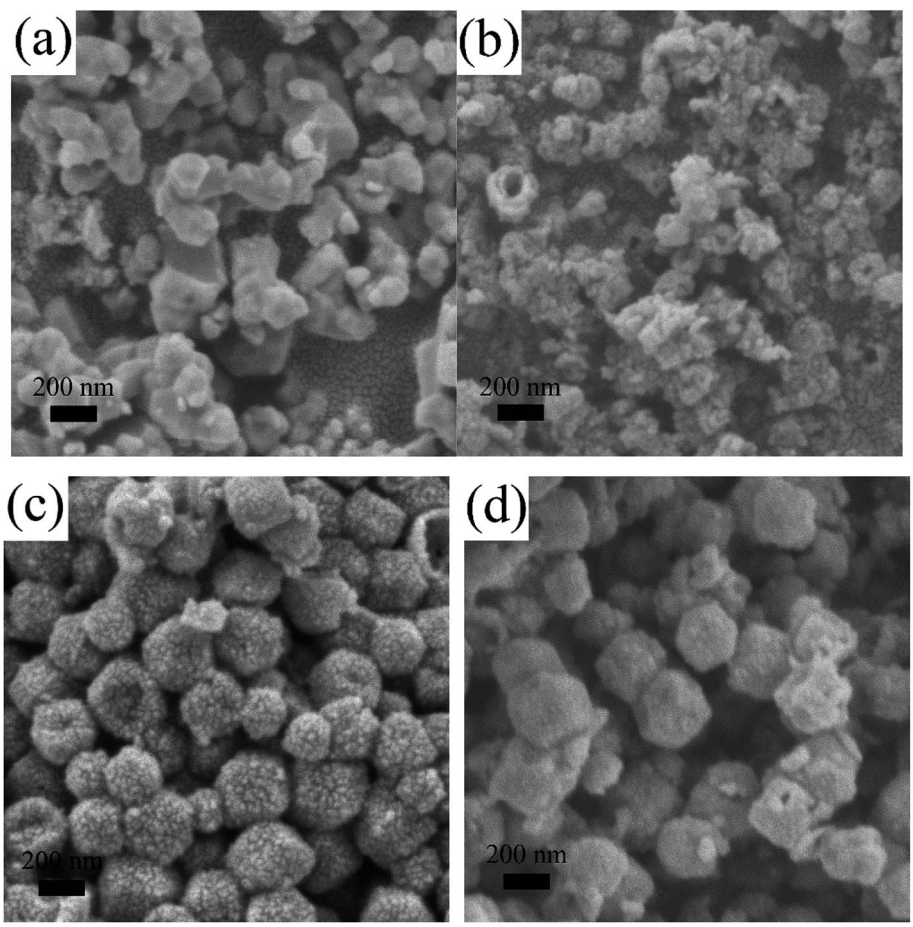

Fig. 3 SEM images of (a) CoS_x, (b) CoS_x/C-1, (c) CoS_x/C-2 and (d) CoS_x/C-3.

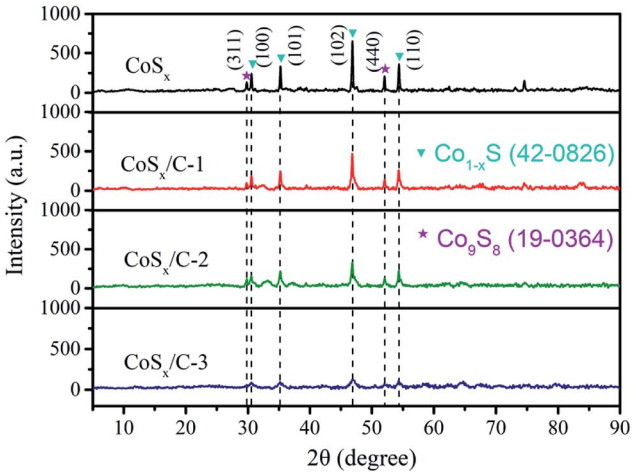

Fig. 4 XRD patterns of CoS_x, CoS_x/C-1, CoS_x/C-2 and CoS_x/C-3.

pentalpha, and the characteristic peaks of the (100), (101), (102) and (110) planes for the $Co_{1-x}S$ (JCPDS card no. 19-0364) at 2θ values of 30.5°, 35.2°, 46.8° and 54.3° are labelled with a blue mark in Fig. 4. On account of the inability to detect the other peaks belonging to crystalline carbon, the carbon was deemed as amorphous. Moreover, with the augment of the carbon content, there was a visible decrease in the intensity of the diffraction peaks from CoS_x/C, which unveiled an obstructive effect on the grain growth of cobalt sulfides by amorphous carbon.[49]

To unearth the precise statistics for the carbon content, TG-DSC was used to interpret CoS_x, CoS_x/C-1, CoS_x/C-2 and CoS_x/C-3 with temperature initiating from 25 °C and ending at 800 °C under the air atmosphere, as revealed in Fig. S2.† Along with the evaporation of water (adsorption from the air), an apparent weight loss was observed from 25 °C to 200 °C. Soon after, the weight loss trend transformed for temperatures higher than 300 °C. As pointed out in a previous research, a series of weight changes can be attributed to the complicated reaction between CoS_x and oxygen, and the further pyrolytic degradation of some intermediate products results in the formation of Co_3O_4.[49] To calculate the carbon content, the temperature of 575 °C was selected as a standard because all the samples temporarily steady in weight and the carbon in the CoS_x/C could react with oxygen to form CO_2. The calculation details are shown in Fig. S2e† and the calculated carbon contents were 2.5%, 5.3% and 11.0% in CoS_x/C-1, CoS_x/C-2 and CoS_x/C-3, respectively.

The microstructures of the CoS_x/C-2 hierarchical hollow nanocages are depicted in detail in Fig. 5a and b. The well-

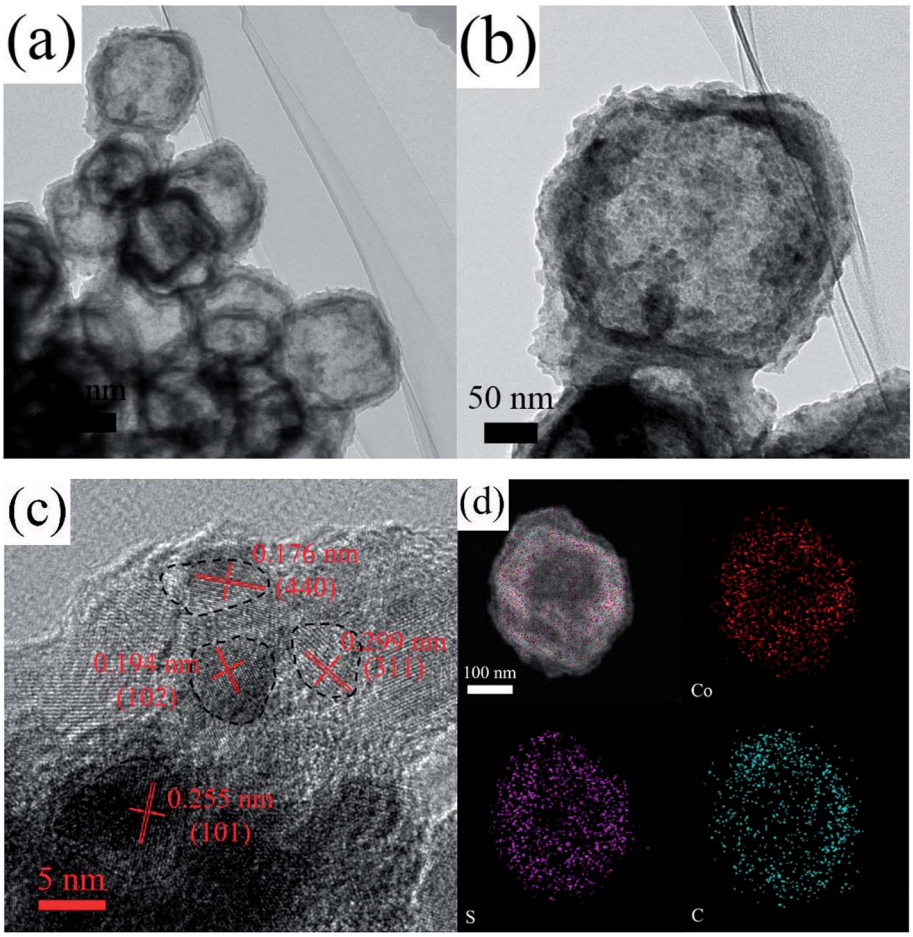

Fig. 5 (a and b) TEM images, (c) HRTEM images and (d) mapping of CoS_x/C-2 hollow nanocages.

defined carbon layer can be clearly seen, which supports the two uniform CoS_x layers consisting of monodispersed nanoparticles with a diameter of *ca.* 10 nm. These outer nanoparticles were consistent with the rough surface of CoS_x/C-2, as shown in Fig. 3c and S1c.† In addition, the composition of CoS_x was assured by the HRTEM lattice image in Fig. 5c. The notable *d*-spacings of 0.176 nm and 0.299 nm were well-substantiated to those of the (440) and (311) planes of Co_9S_8, and the *d*-spacings of 0.194 nm and 0.255 nm corroborated to with those of the (102) and (101) planes of $Co_{1-x}S$, which agreed well with the XRD pattern (Fig. 4).[44] The elemental mapping of a single CoS_x/C-2 hierarchical hollow nanocage confirmed the uniform presence of Co, S and C throughout the surface of the sample, as given in Fig. 5d. In addition, the atomic ratio of S and Co was 1.08 in this single hollow nanocages.

The electrochemical performance of the as-prepared CoS_x/C electrode was evaluated using cyclic voltammetry (CV) and galvanostatic charge/discharge cycling with the assistance of a three-electrode system in an aqueous electrolyte containing 1 M KOH. Fig. 6a exhibits the CV curves of the CoS_x/C-2 hollow nanocages at various scan rates from 5 mV s^{-1} to 100 mV s^{-1} within the potential window from 0 V to 0.5 V (*vs.* saturated calomel electrode, SCE). Apparently, the ampere density was gradually augmented along with the scan rate as the shape of the CV curve was well-preserved without any marked deformation. When the scan rate reached 5 mV s^{-1}, the oxidation and reduction peaks were around 0.36 V and 0.29 V, respectively. The anodic peaks shifted in the anodic direction, while the cathodic peaks tended to shift in the opposite direction. Similar to the CV curves for CoS_x (Fig. S3a†), all of the curves for CoS_x/C-1 (Fig. S3b†) and CoS_x/C-2 (Fig. S3c†) presented a clear pseudo capacitance featured with an unchanged shape. According to previous reports, the faradaic reactions with the incorporation of the cobalt sulfide-based materials in the alkaline solution system are shown in eqn (1) and (2).[50–52] From the data in Fig. 6a, it is apparent that a pair of redox peaks (A2 and C2) associated with eqn (2) were highly reversible, while in the other pair of redox peaks (A1 and C1) the reduction peak C1 was almost invisible. This finding indicates that the reaction given in eqn (1) tends to mostly oxidize, which aligns well with the previous report.[50] In particular, the curves of the CoS_x/C-2 hollow nanocages still maintained a regular shape with much slighter peaks shifts than those of CoS_x. This result occurred even though the scan rate is increased to 100 mV s^{-1}, thus attesting the promotion to a fast redox reaction from the appropriate incorporation of the carbon layer. The comparison of the CV curves for CoS_x, CoS_x/C-1, CoS_x/C-2 and CoS_x/C-3 at 10 mV s^{-1} is shown in Fig. S3d.† The relatively higher area of the closed CV curve for the CoS_x/C-2 hollow nanocages surmised higher reactivities for the redox reactions. Within the potential

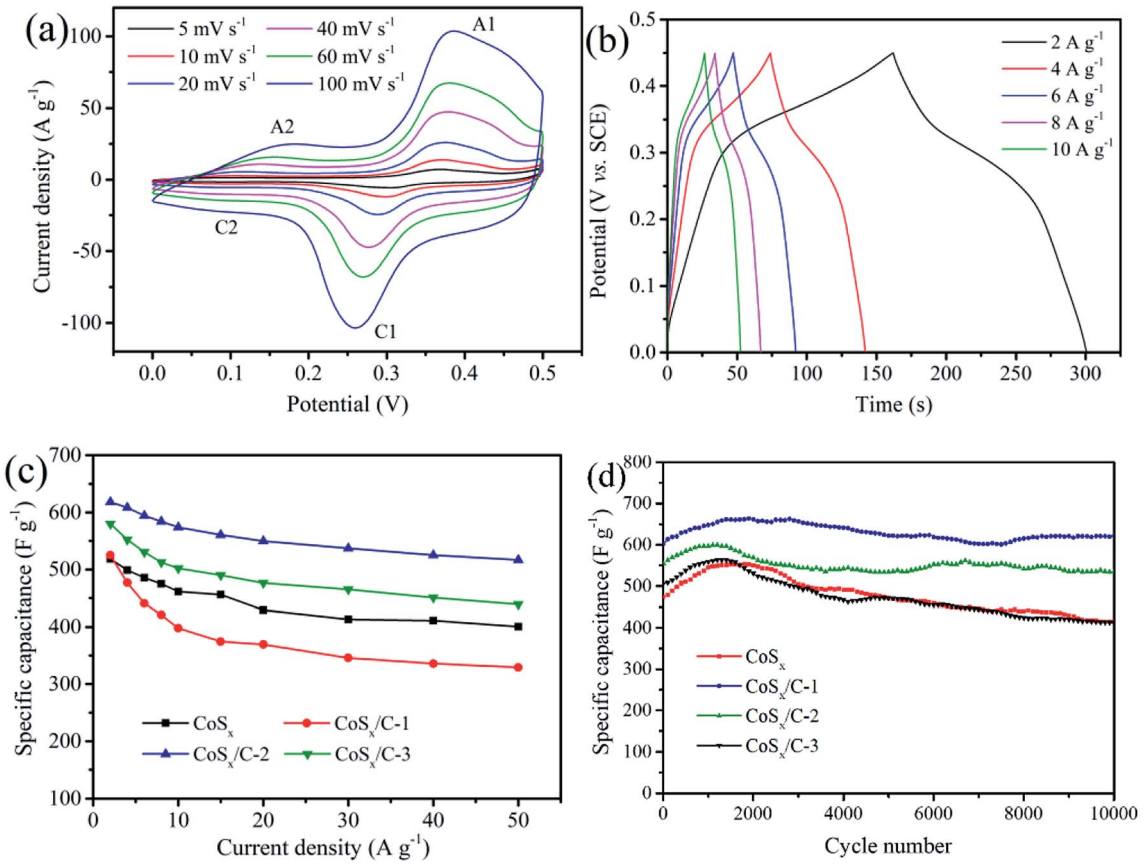

Fig. 6 (a) CV curves and (b) galvanostatic charge–discharge curves of CoS_x/C-2 hollow nanocages. (c) Rate performance and (d) cycling performance of CoS_x, CoS_x/C-1, CoS_x/C-2 and CoS_x/C-3.

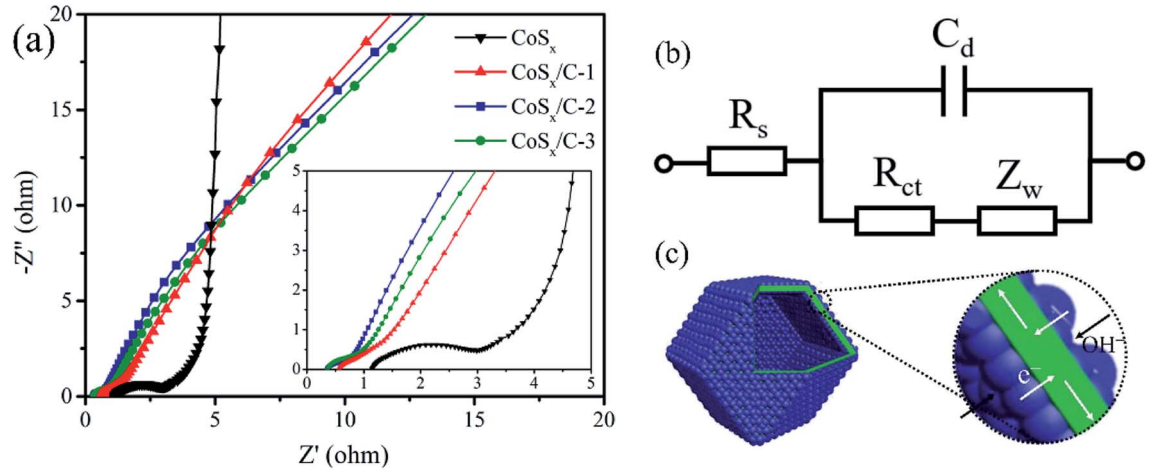

Fig. 7 (a) EIS spectra and (b) equivalent circuits of CoS_x, CoS_x/C-1, CoS_x/C-2 and CoS_x/C-3. (c) Schematic models of the charge transfer and ion diffusion path of CoS_x/C hollow nanocages.

window of 0 V to 0.45 V at various current densities, the galvanostatic charge–discharge investigation was disseminated to measure the specific capacitances of all specimens, as shown in Fig. 6b and S4.† The CoS_x/C-2 hollow nanocages exhibited admirable specific capacitances of 618.4 F g^{-1}, 608.4 F g^{-1}, 594.4 F g^{-1}, 584.3 F g^{-1} and 574.1 F g^{-1} at discharge current densities of 2 A g^{-1}, 4 A g^{-1}, 6 A g^{-1}, 8 A g^{-1}, and 10 A g^{-1}, respectively, which exceeded those of the pristine CoS_x (Fig. S4a†) (518.6 F g^{-1}, 498.7 F g^{-1}, 485.6 F g^{-1}, 474.9 F g^{-1} and 461.3 F g^{-1} at the corresponding current densities). A comparison of the rate performance for all the samples is given in Fig. 6c, the specific capacitance of the CoS_x/C-2 hollow nanocages was retained as high as 83.6% with the current density ranging from 2 A g^{-1} to 50 A g^{-1}.

$$CoS_x + OH^- \leftrightarrow CoS_xOH + e^- \quad (1)$$

$$CoS_xOH + OH^- \leftrightarrow CoS_xO + H_2O + e^- \quad (2)$$

This superior rate performance should be ascribed to the optimized charge transfer procedure, which is expounded by the EIS spectra and the corresponding equivalent circuit in Fig. 7. The resistance of the system (R_s), consisting of the ohmic resistance of the aqueous electrolyte, the electrolyte/electrode interface and active materials, was 0.33 Ω for the CoS_x/C-2 hollow nanocages and 1.30 Ω for pristine CoS_x. The R_s values for CoS_x/C-1 and CoS_x/C-3 was also smaller than that for pristine CoS_x as shown in the magnified EIS spectra (inset, Fig. 7a), confirming that the interior high-conductivity carbon layer can effectively diminish the R_s. The charge transference resistance (R_{ct}) of the CoS_x/C-2 hollow nanocages with the incorporation of the carbon layer was dramatically decreased to 0.68 Ω compared to that of pristine CoS_x (2.36 Ω). The decline in the R_{ct} value also appeared for CoS_x/C-1 (2.01 Ω) and CoS_x/C-3 (0.86 Ω), revealing that the interior high-conductivity of the carbon layer can effectively diminish the charge transfer resistance. The schematic in Fig. 7c discloses the decreased charge transfer and improved the ion diffusion path for the CoS_x/C-2 hollow nanocages. Moreover, the carbon layer of high-conductivity could effectively get the charges from the cobalt sulfide nanoparticles attached on the both side of the layer, which donated the unique charge transfer path compared to the aggregated regular CoS_x. The hollow structure and cobalt sulfide nanoparticles enlarged the contact area between the electrolyte and electrode materials, providing more active redox sites in comparison to the aggregated pristine CoS_x.[53,54] These two factors were mainly responsible for the increased specific capacitance and enhanced rate performance. It is believed that the rational hierarchical hollow nanocages containing the high-conductive carbon layer support can be useful in boosting the electrochemical performance of more electrode materials.

Table 1 The electrochemical performance of reported cobalt sulfides materials as an electrode for supercapacitors

Material	Specific capacitance (F g^{-1})	Cycling performance	Reference
Co_xS@PC/rGO	455.0 (2 A g^{-1})	99.7% (4000 cycles, 1 A g^{-1})	43
CoSNC	360 (1.5 A g^{-1})	90% (2000 cycles, 12 A g^{-1})	55
Co_9S_8/GPs	536 (1 A g^{-1})	91.8% (2500 cycles, 10 A g^{-1})	56
Co_9S_8@C	514 (1 A g^{-1})	88% (1000 cycles, 8 A g^{-1})	57
Co_9S_8 nanotubes	285.3 (2 A g^{-1})	90.4% (1000 cycles, 2 A g^{-1})	50
Co_9S_8 nanospheres	306.1 (0.1 A g^{-1})	—	58
3D flower-like Co_9S_8	522 (0.5 A g^{-1})	97.7% (1000 cycles, 1 A g^{-1})	51
CoS_x/C-2	618.4 F g^{-1} (2 A g^{-1})	*ca.* 100% (10 000 cycles, 4 A g^{-1})	This study

The cycling performance of the CoS_x/C-2 hollow nanocage electrode was also analyzed *via* galvanostatic charge–discharge tests for 10 000 cycles when the current density was 4.0 A g^{-1}, as exhibited in Fig. 6d. The specific capacitances of all the samples were elevated at the very beginning due to the activation of CoS_x,[43,50] then decreased to some content and later stabilized. After 10 000 cycles, the high specific capacitances of the CoS_x/C-2 hollow nanocages were still retained without any evident capacity fading. The high specific capacitances were much better than that of the pristine CoS_x (*ca.* 81.6%), CoS_x/C-1 (*ca.* 87.6%) and CoS_x/C-3 (*ca.* 94.7%), proving the long-term electrochemical stability of the hierarchical hollow nanocages. It should be noted that the hierarchically hollow structure was composed of a carbon layer framework and nano-sized cobalt sulfide particles, which maintained the morphology stability, prevented aggregation and eliminated deactivation during the iterative redox reactions. Recent reports on the use of cobalt sulfides as electrode materials for supercapacitors are enumerated in Table 1. Our optimized CoS_x/C hierarchical hollow nanocages demonstrated an excellent electrochemical performance compared to previous works.[39–42,50,51,55–58]

4. Conclusion

In summary, cobalt sulfide hierarchical hollow nanocages coated with a carbon layer were synthesized using ZIF-67 nanocrystals coated with RF as a self-sacrificial template. The morphology and electrochemical performance was investigated for the CoS_x/C hierarchical hollow nanocages with different carbon contents of the RF coating layer after an *in situ* transformation to a conductive carbon layer. The results demonstrated that an appropriate RF coating layer could promote the formation of hollow nanocages. The modified CoS_x/C hierarchical hollow nanocages demonstrated a superior rate performance (83.6% capacitance retention with a current density varying from 2 A g^{-1} to 50 A g^{-1}) and an extraordinary cycling durability without the capacity fading after 10 000 cycles. The prominent electrochemical performance could be ascribed to the elaborately designed hierarchical hollow structure, which provided support and protection for the hollow shells and the conductive carbon layer. This technique could be generally extended to other related materials, such as various MOFs.

Conflicts of interest

There are no conflicts to declare.

Acknowledgements

This work was supported by the Key Project of MOST (2016YFB0700600), the National Natural Science Foundation Committee of China (Distinguished Youth Scientists Project of 51425301, U1601214, 51573013, 51773092 and 51772147), the 1000 Youth Talents Plan of the National Natural Science Foundation of China (51773092), the Research Foundation of State Key Lab (ZK201805 and ZK201717) and the Jiangsu Distinguished Professorship Program (2016).

References

1 F. Wang, X. Wu, X. Yuan, Z. Liu, Y. Zhang, L. Fu, Y. Zhu, Q. Zhou, Y. Wu and W. Huang, Latest advances in supercapacitors: from new electrode materials to novel device designs, *Chem. Soc. Rev.*, 2017, **46**, 6816–6854.
2 M. Winter and R. J. Brodd, What are batteries, fuel cells, and supercapacitors?, *Chem. Rev.*, 2004, **104**, 4245–4269.
3 G. Wang, L. Zhang and J. Zhang, A review of electrode materials for electrochemical supercapacitors, *Chem. Soc. Rev.*, 2012, **41**, 797–828.
4 P. Simon, Y. Gogotsi and B. Dunn, Where do batteries end and supercapacitors begin?, *Science*, 2014, **343**, 1210–1211.
5 B. E. Conway, V. Birss and J. Wojtowicz, The role and utilization of pseudocapacitance for energy storage by supercapacitors, *J. Power Sources*, 1997, **66**, 1–14.
6 L. L. Zhang and X. S. Zhao, Carbon-based materials as supercapacitor electrodes, *Chem. Soc. Rev.*, 2009, **38**, 2520–2531.
7 Y. Zhu, S. Murali, M. D. Stoller, K. J. Ganesh, W. Cai, P. J. Ferreira, A. Pirkle, R. M. Wallace, K. A. Cychosz and M. Thommes, Carbon-based supercapacitors produced by activation of graphene, *Science*, 2011, **332**, 1537–1541.
8 E. Frackowiak, Carbon materials for supercapacitor application, *Phys. Chem. Chem. Phys.*, 2007, **9**, 1774–1785.
9 G. A. Snook, P. Kao and A. S. Best, Conducting-polymer-based supercapacitor devices and electrodes, *J. Power Sources*, 2011, **196**, 1–12.
10 C. Meng, C. Liu, L. Chen, C. Hu and S. Fan, Highly flexible and all-solid-state paperlike polymer supercapacitors, *Nano Lett.*, 2010, **10**, 4025–4031.
11 X. Lang, A. Hirata, T. Fujita and M. Chen, Nanoporous metal/oxide hybrid electrodes for electrochemical supercapacitors, *Nat. Nanotechnol.*, 2011, **6**, 232.
12 P. Zhang, X. Zhao, Z. Liu, F. Wang, Y. Huang, H. Li, Y. Li, J. Wang, Z. Su, G. Wei, Y. Zhu, L. Fu, Y. Wu and W. Huang, Exposed high-energy facets in ultradispersed sub-10 nm SnO_2 nanocrystals anchored on graphene for pseudocapacitive sodium storage and high-performance quasi-solid-state sodium-ion capacitors, *NPG Asia Mater.*, 2018, **10**, 429–440.
13 C. Wei, R. Zhang, X. Zheng, Q. Ru, Q. Chen, C. Cui, G. Li and D. Zhang, Hierarchical porous $NiCo_2O_4$/CeO_2 hybrid materials for high performance supercapacitors, *Inorg. Chem. Front.*, 2018, **5**, 3126–3134.
14 X.-Y. Yu, L. Yu and X. W. D. Lou, Metal sulfide hollow nanostructures for electrochemical energy storage, *Adv. Energy Mater.*, 2016, **6**, 1501333.
15 L. Shen, L. Yu, H. B. Wu, X.-Y. Yu, X. Zhang and X. W. D. Lou, Formation of nickel cobalt sulfide ball-in-ball hollow spheres with enhanced electrochemical pseudocapacitive properties, *Nat. Commun.*, 2015, **6**, 6694.
16 Y. M. Chen, Z. Li and X. W. D. Lou, General formation of $M_xCo_{3-x}S_4$(M= Ni, Mn, Zn) hollow tubular structures for hybrid supercapacitors, *Angew. Chem.*, 2015, **127**, 10667–10670.

17 C. Z. Wei, Q. L. Ru, X. T. Kang, H. Y. Hou, C. Cheng and D. J. Zhang, Self-template synthesis of double shelled ZnS-$NiS_{1.97}$ hollow spheres for electrochemical energy storage, *Appl. Surf. Sci.*, 2018, **435**, 993–1001.

18 T. Cottineau, M. Toupin, T. Delahaye, T. Brousse and D. Bélanger, Nanostructured transition metal oxides for aqueous hybrid electrochemical supercapacitors, *Appl. Phys. A*, 2006, **82**, 599–606.

19 Z. Fan, D. Qi, Y. Xiao, J. Yan and T. Wei, One-step synthesis of biomass-derived porous carbon foam for high performance supercapacitors, *Mater. Lett.*, 2013, **101**, 29–32.

20 K. H. An, W. S. Kim, Y. S. Park, Y. C. Choi, S. M. Lee, D. C. Chung, D. J. Bae, S. C. Lim and Y. H. Lee, Supercapacitors using single-walled carbon nanotube electrodes, *Adv. Mater.*, 2001, **13**, 497–500.

21 C. Wei, N. Zhan, J. Tao, S. Pang, L. Zhang, C. Cheng and D. Zhang, Synthesis of hierarchically porous $NiCo_2S_4$ core-shell hollow spheres via self-template route for high performance supercapacitors, *Appl. Surf. Sci.*, 2018, **453**, 288–296.

22 C. H. Lai, M. Y. Lu and L. J. Chen, Metal sulfide nanostructures: synthesis, properties and applications in energy conversion and storage, *J. Mater. Chem.*, 2012, **22**, 19–30.

23 J. Yang, X. Duan, Q. Qin and W. Zheng, Solvothermal synthesis of hierarchical flower-like β-NiS with excellent electrochemical performance for supercapacitors, *J. Mater. Chem. A*, 2013, **1**, 7880–7884.

24 J. Shi, X. Li, G. He, L. Zhang and M. Li, Electrodeposition of high-capacitance 3D CoS/graphene nanosheets on nickel foam for high-performance aqueous asymmetric supercapacitors, *J. Mater. Chem. A*, 2015, **3**, 20619–20626.

25 W. Xia, A. Mahmood, R. Zou and Q. Xu, Metal–organic frameworks and their derived nanostructures for electrochemical energy storage and conversion, *Energy Environ. Sci.*, 2015, **8**, 1837–1866.

26 S. Bai, X. Liu, K. Zhu, S. Wu and H. Zhou, Metal–organic framework-based separator for lithium–sulfur batteries, *Nat. Energy*, 2016, **1**, 16094.

27 F. Zheng, Y. Yang and Q. Chen, High lithium anodic performance of highly nitrogen-doped porous carbon prepared from a metal-organic framework, *Nat. Commun.*, 2014, **5**, 5261.

28 S. L. James, Metal-organic frameworks, *Chem. Soc. Rev.*, 2003, **32**, 276–288.

29 H. Li, M. Eddaoudi, M. O'Keeffe and O. M. Yaghi, Design and synthesis of an exceptionally stable and highly porous metal-organic framework, *Nature*, 1999, **402**, 276.

30 B. Liu, H. Shioyama, H. Jiang, X. Zhang and Q. Xu, Metal–organic framework (MOF) as a template for syntheses of nanoporous carbons as electrode materials for supercapacitor, *Carbon*, 2010, **48**, 456–463.

31 R. Díaz, M. G. Orcajo, J. A. Botas, G. Calleja and J. Palma, Co8-MOF-5 as electrode for supercapacitors, *Mater. Lett.*, 2012, **68**, 126–128.

32 F. Yu, Z. Chang, X. Yuan, F. Wang, Y. Zhu, L. Fu, Y. Chen, H. Wang, Y. Wu and W. Li, Ultrathin $NiCo_2S_4$@graphene with a core-shell structure as a high performance positive electrode for hybrid supercapacitors, *J. Mater. Chem. A*, 2018, **6**, 5856–5861.

33 H. Hu, B. Y. Guan and X. W. Lou, Construction of complex CoS hollow structures with enhanced electrochemical properties for hybrid supercapacitors, *Chem*, 2016, **1**, 102–113.

34 C. Yuan, L. Yang, L. Hou, J. Li, Y. Sun, X. Zhang, L. Shen, X. Lu, S. Xiong and X. W. D. Lou, Flexible hybrid paper made of monolayer Co_3O_4 microsphere arrays on rGO/CNTs and their application in electrochemical capacitors, *Adv. Funct. Mater.*, 2012, **22**, 2560–2566.

35 Z. Chen, V. Augustyn, J. Wen, Y. Zhang, M. Shen, B. Dunn and Y. Lu, High-performance supercapacitors based on intertwined CNT/V_2O_5 nanowire nanocomposites, *Adv. Mater.*, 2011, **23**, 791–795.

36 J. Y. Lee, K. Liang, K. H. An and Y. H. Lee, Nickel oxide/carbon nanotubes nanocomposite for electrochemical capacitance, *Synth. Met.*, 2005, **150**, 153–157.

37 M. Zhi, C. Xiang, J. Li, M. Li and N. Wu, Nanostructured carbon–metal oxide composite electrodes for supercapacitors: a review, *Nanoscale*, 2013, **5**, 72–88.

38 X. Wang, M. Li, Z. Chang, Y. Yang, Y. Wu and X. Liu, Co_3O_4@MWCNT nanocable as cathode with superior electrochemical performance for supercapacitors, *ACS Appl. Mater. Interfaces*, 2015, **7**, 2280–2285.

39 T. Zhu, B. Xia, L. Zhou and X. W. D. Lou, Arrays of ultrafine CuS nanoneedles supported on a CNT backbone for application in supercapacitors, *J. Mater. Chem.*, 2012, **22**, 7851–7855.

40 T. Zhu, H. B. Wu, Y. Wang, R. Xu and X. W. D. Lou, Formation of 1D hierarchical structures composed of Ni_3S_2 nanosheets on CNTs backbone for supercapacitors and photocatalytic H_2 production, *Adv. Energy Mater.*, 2012, **2**, 1497–1502.

41 H. Zhang, X. Yu, D. Guo, B. Qu, M. Zhang, Q. Li and T. Wang, Synthesis of bacteria promoted reduced graphene oxide-nickel sulfide networks for advanced supercapacitors, *ACS Appl. Mater. Interfaces*, 2013, **5**, 7335–7340.

42 A. Mohammadi, N. Arsalani, A. G. Tabrizi, S. E. Moosavifard, Z. Naqshbandi and L. S. Ghadimi, Engineering rGO-CNT wrapped Co_3S_4 nanocomposites for high-performance asymmetric supercapacitors, *Chem. Eng. J.*, 2018, **334**, 66–80.

43 Y. Wang, B. Chen, Z. Chang, X. Wang, F. Wang, L. Zhang, Y. Zhu, L. Fu and Y. Wu, Enhancing performance of sandwich-like cobalt sulfide and carbon for quasi-solid-state hybrid electrochemical capacitors, *J. Mater. Chem. A*, 2017, **5**, 8981–8988.

44 P. Wang, C. Li, W. Wang, J. Wang, Y. Zhu and Y. Wu, Hollow Co_9S_8 from metal organic framework supported on rGO as electrode material for highly stable supercapacitors, *Chin. Chem. Lett.*, 2018, **29**, 612–615.

45 S. Dong, C. Li, X. Ge, Z. Li, X. Miao and L. Yin, ZnS-Sb_2S_3@C core-double shell polyhedron structure derived from metal-organic framework as anodes for high performance sodium ion batteries, *ACS Nano*, 2017, **11**, 6474–6482.

46 C. Li, W. Wu, P. Wang, W. Zhou, J. Wang, Y. Chen, L. Fu, Y. Zhu, Y. Wu and W. Huang, Fabricating an aqueous symmetric supercapacitor with a stable high working voltage of 2 V by using an alkaline–acidic electrolyte, *Adv. Sci.*, 2018, 1801665.

47 J. Qian, F. Sun and L. Qin, Hydrothermal synthesis of zeolitic imidazolate framework-67(ZIF-67) nanocrystals, *Mater. Lett.*, 2012, **82**, 220–223.

48 Z. Jiang, W. Lu, Z. Li, K. H. Ho, X. Li, X. Jiao and D. Chen, Synthesis of amorphous cobalt sulfide polyhedral nanocages for high performance supercapacitors, *J. Mater. Chem. A*, 2014, **2**, 8603–8606.

49 X. Liu, H. Liu, Y. Zhao, Y. Dong, Q. Fan and Q. Kuang, Synthesis of the carbon-coated nanoparticle Co_9S_8 and its electrochemical performance as an anode material for sodium-ion batteries, *Langmuir*, 2016, **32**, 12593–12602.

50 J. Yu, H. Wan, J. Jiang, Y. Ruan, L. Miao, L. Zhang, D. Xia and K. Xu, Activation mechanism study of dandelion-like Co_9S_8 nanotubes in supercapacitors, *J. Electrochem. Soc.*, 2014, **161**, A996–A1000.

51 L. Yin, L. Wang, X. Liu, Y. Gai, L. Su, B. Qu and L. Gong, Ultra-fast microwave synthesis of 3D flower-Like Co_9S_8 hierarchical architectures for high-performance supercapacitor applications, *Eur. J. Inorg. Chem.*, 2015, 2457–2462.

52 T.-W. Lin, C.-S. Dai, T.-T. Tasi, S.-W. Chou, J.-Y. Lin and H.-H. Shen, High-performance asymmetric supercapacitor based on Co_9S_8/3D graphene composite and graphene hydrogel, *Chem. Eng. J.*, 2015, **279**, 241–249.

53 S. Peng, L. Li, H. B. Wu, S. Madhavi and X. W. D. Lou, Controlled Growth of $NiMoO_4$ Nanosheet and Nanorod Arrays on Various Conductive Substrates as Advanced Electrodes for Asymmetric Supercapacitors, *Adv. Energy Mater.*, 2015, **5**, 1401172.

54 G. Wang, L. Zhang and J. Zhang, A review of electrode materials for electrochemical supercapacitors, *Chem. Soc. Rev.*, 2012, **41**, 797–828.

55 F. Cao, M. Zhao, Y. Yu, B. Chen, Y. Huang, J. Yang, X. Cao, Q. Lu, X. Zhang and Z. Zhang, Synthesis of two-dimensional $CoS_{1.097}$/nitrogen-doped carbon nanocomposites using metal–organic framework nanosheets as precursors for supercapacitor application, *J. Am. Chem. Soc.*, 2016, **138**, 6924–6927.

56 D. Xiong, X. Li, Z. Bai, J. Li, Y. Han and D. Li, Vertically aligned Co_9S_8 nanotube arrays onto graphene papers as high-performance flexible electrodes for supercapacitors, *Chem.–Eur. J.*, 2018, **24**, 2339–2343.

57 T. W. Lin, H. C. Tsai, T. Y. Chen and L. D. Shao, Facile and controllable one-pot synthesis of hierarchical Co_9S_8 hollow microspheres as high-performance electroactive materials for energy storage and conversion, *ChemElectroChem*, 2018, **5**, 137–143.

58 L. Zhang, Y. Wang, W. Zhou, G. Song and S. Cheng, Facile synthesis of hollow Co_9S_8 nanospheres for high performance pseudocapacitor, *Int. J. Electrochem. Sci.*, 2016, **11**, 1541–1548.

